Turk J Elec Engin, VOL.10, NO.2 2002, © TÜBİTAK

# Two-Dimensional Photonic Crystal L-Shaped Bent Waveguide and its Application to Wavelength Multi/Demultiplexer

**Yoshihiro NAKA and Hiroyoshi IKUNO**
*Department of Electrical and Computer Engineering, Kumamoto University*
*Kurokami 2-39-1, Kumamoto-shi, 860-8555 JAPAN*
*e-mail: naka@eecs.kumamoto-u.ac.jp, ikuno@eecs.kumamoto-u.ac.jp*

**Abstract**

*The bent waveguide is a key element for integrated optical signal processing waveguide devices. We propose a new type of two-dimensional photonic crystal L-shaped bent waveguides with additional pillars at the corner. Using the FDTD method based on the principle of multidimensional wave digital filters we simulate its transmission characteristics and show an excellent transmission of light in L-shaped bent waveguide. As an application we design compact size multi/demultiplexer composed of the L-shaped bent waveguides and directional couplers and realize multi/demultiplexer with low-insertion loss and high extinction ratio device whose size is of the order of the wavelength of light.*

**Key Words:** *photonic crystals, L-shaped bent wave guide, multi/demultiplexer, FDTD, multidimensional wave digital filters*

## 1. Introduction

Great interests have been given to the photonic crystal whose photonic band gap has attracted considerable possibility [1, 2]. By using the strong confinement of the light by the photonic band gap, it is expected that waveguide devices whose size is of the order of the wavelength of light can be realized [2]. In fact, several microscale photonic crystal optical waveguide devices have been proposed [3, 4, 5, 6, 7, 8]. It is important for designing high density integrated optical devices to clarify fundamental properties of basic photonic crystal waveguides such as straight waveguide, right-angle bent waveguide, directional coupler, and so on [5, 6, 7]. Particularly, we need to develop highly efficient transmission devices such as L-shaped bent waveguides in order to realize compact integrated optical circuits.

In this paper we propose an L-shaped bent waveguide with excellent transmission characteristics as shown in Figure 1: the right-angle bent waveguide has additional pillars at the corner which act as potential barriers making a resonant tunneling in a quantum wire [5, 9]. The photonic crystal employed here is composed of circular dielectric pillars in air on a square array. Using the L-shaped bent waveguide we design compact size multi/demultiplexer. First, we analyze characteristics of the L-shaped bent waveguide using the finite-difference time-domain (FDTD) method based on the principles of multidimensional wave digital filters (MD-WDFs) [10, 11]; this method [5, 12] can easily be implemented and is more accurate than the conventional one, the Yee algorithm. We show that reflected waves from the right-angle corner can be

completely eliminated by adding additional pillars due to resonant tunneling and its transmission bandwidths can be controlled by changing parameters of additional pillars. Using the L-shaped bent waveguides together with the several numbers of directional couplers, we design the multi/demultiplexer and demonstrate that it can work as low-insertion-loss device whose size is of the order of the wavelength of light.

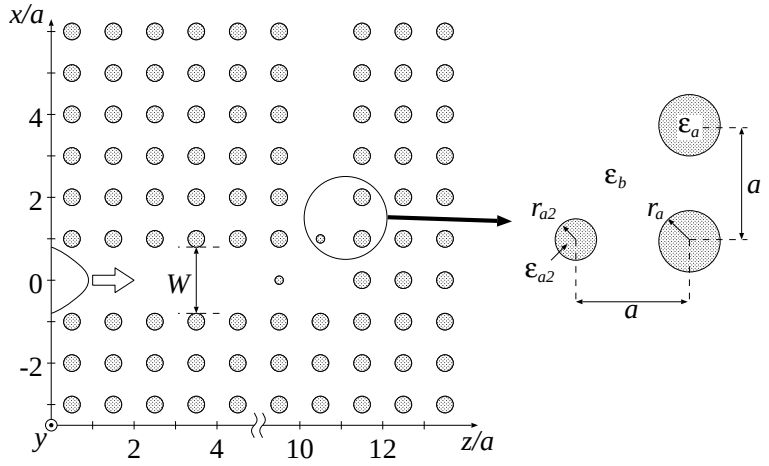


**Figure 1.** Photonic crystal L-shaped bend waveguide with additional pillars in the corner region.

## 2. Novel L-Shaped Bent Waveguide

We consider a two-dimensional photonic crystal L-shaped bent waveguide with additional dielectric pillars in the corner region as shown in Figure 1. Photonic crystals used here is composed of circular dielectric pillars in air on a square array with lattice constant $a$. The optical waveguide can be created by removing one row of pillars. The optical light is confined in the defect when incident frequency is inside the photonic band gap, because electromagnetic field cannot propagate in the photonic crystal which works as cladding layers. The relative permittivity of the pillars and background are $\varepsilon_a = 11.56$ and $\varepsilon_b = 1.0$, respectively. In order to obtain a wide range of photonic band gap, we choose the radii of pillars as $r_a/a = 0.175$. The waveguide width is $W/a = 1.65$ to keep single mode propagation. In the corner region two additional dielectric pillars are placed whose radii and relative permittivity are $r_{a2}$ and $\varepsilon_{a2}$, respectively. The photonic crystal has a band gap for $E$ polarized field $(E_y, H_x, H_z)$ whose frequency range is extended from $0.320(= \omega a/2\pi c)$ to $0.462$, where $c$ is the speed of light in a vacuum, while there is no photonic band gap for $H$ polarized field. The incident pulse is taken as

$$\psi(x, z = 0, t) = \psi_0(x) \exp\left(\frac{t - t_0}{T}\right)^2 \sin\left\{\omega_c(t - t_0)\right\}, \tag{1}$$

where $\psi_0(x)$ denotes a transverse profile which is a truncated cosine, $T$ is a pulse duration, $t_0$ is a center point of the incident pulse, and $\omega_c$ is a center angular frequency. By taking into account a propagation constant of fundamental mode in the straight photonic crystal waveguides (see the Appendix), the parameters of incident wave $\omega_c a/2\pi c = 0.40$ and $cT/a = 11.0$ are chosen.

Method of solution employed here is the FDTD method based on the principles of MD-WDFs because of the accuracy and stability on its algorithm [5, 12]. The perfectly matched layers (PMLs) [13] are used as the absorbing boundary condition at the edges of computational zone. Taking impedance matching condition

at the interface between the computational region and PMLs region into account, in the PMLs region we use the same waveguide structure as that of computational region, but electric conductivity and magnetic loss are assigned to dielectric material whose value satisfies the distortion-less condition [13]. The square grid space cells $\delta = \delta x = \delta z = a/20$ and the time step $c\delta t = 0.5\delta$ are used.

Figure 2 shows a Poynting vector and electric field intensity of an L-shaped bent waveguide at the resonant frequency $\omega a/2\pi c = 0.389$. The radii and relative permittivity of the additional pillars are $r_{a2}/a = 0.175$ and $\varepsilon_{a2} = 11.56$, respectively. We can see that optical power efficiently flows through right-angle bend and electric field concentrates at corner region due to resonant tunneling.

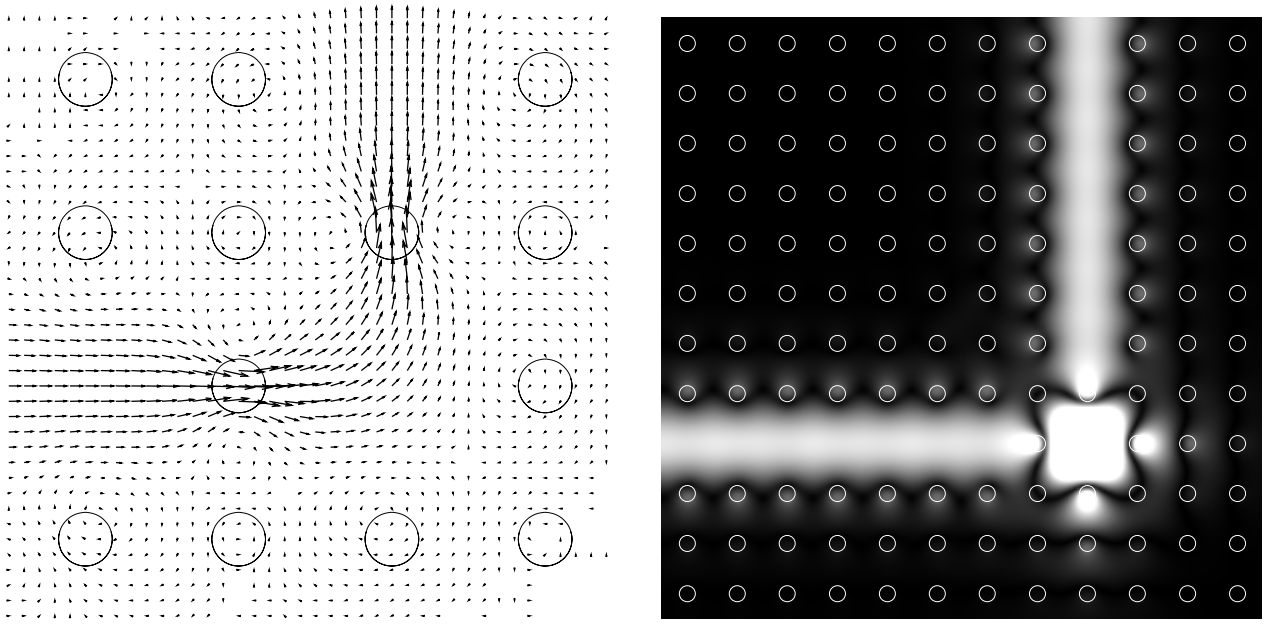

(a) (b)

**Figure 2.** Poynting vector and electric field intensity of L-shaped bent waveguide at the resonant frequency $\omega a/2\pi c = 0.389$. The radii and relative permittivity of additional pillars are $r_{a2}/a = 0.175$ and $\varepsilon_{a2} = 11.56$, respectively. (a) Poynting vector. (b) Electric field intensity.

Figure 3 shows optical power transmission characteristics when radii and relative permittivity of additional pillars are changed. The power flow in the waveguide is defined by

$$P = -\int_S \langle \boldsymbol{E} \times \boldsymbol{H} \rangle \cdot \boldsymbol{e}_\alpha \, dS \tag{2}$$

where $S$ means cross section of the waveguide, $\langle \cdot \rangle$ denote time average operator, and $\boldsymbol{e}_\alpha, \alpha = x, z$ are unit vectors of propagation direction. By adding additional pillars we can completely eliminate reflected waves from the right-angle corner at the resonant frequency. We can see from Figure 3a that for an increase of radii $r_{a2}$ the resonant frequency shifts to a lower side and its quality factor increases. We can see from Figure 3b that increasing relative permittivity $\varepsilon_{a2}$ shows same effect as that arises when radii $r_{a2}$ are changed. Resonant frequencies as a function of relative permittivity $\varepsilon_{a2}$ of additional pillars are shown in Figure 4. The radii of additional pillars $r_{a2}/a = 0.175$ are fixed. Error bars in the figure indicate transmission bandwidths whose reflected power loss at the corner are less than 0.2 dB. This figure shows that we can control transmission frequency ranges by changing relative permittivity of additional pillars.

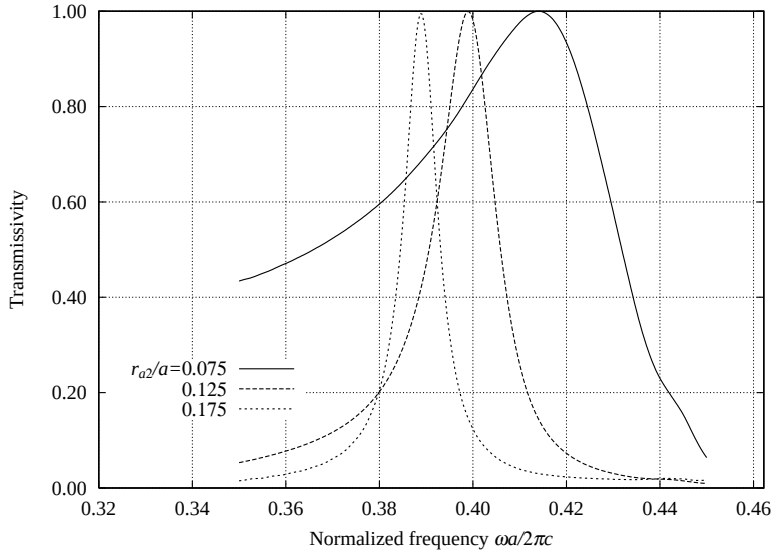


(a)

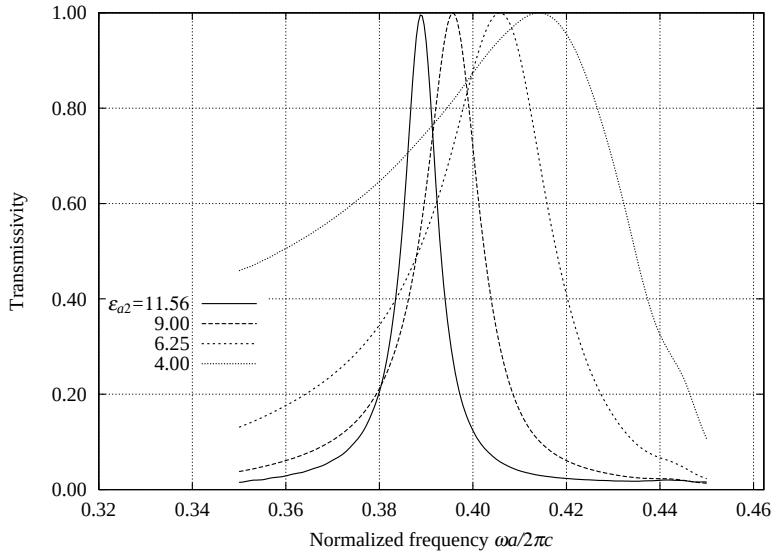


(b)

**Figure 3.** Optical power transmission characteristics of L-shaped bent waveguide when the radii $r_{a2}$ and relative permittivity $\varepsilon_{a2}$ of additional pillars are changed. (a) The radii $r_{a2}$ are changed. ($\varepsilon_{a2} = 11.56$) (b) The relative permittivity $\varepsilon_{a2}$ are changed. ($r_{a2}/a = 0.175$)

Next, we evaluate mode field profiles in the L-shaped bent waveguide by comparing those of input and output waveguide. Figure 5 shows spatial profile of electric field intensities $|E_y|$ as a function of propagation constant $\beta a/2\pi$ for input side and output side of the L-shaped bent waveguide at the resonant frequency $\omega a/2\pi c = 0.389$. In the input side of the waveguide we can find that there are no reflected waves and confirm the formation of eigenmode which is the same as in the straight photonic crystal waveguide (See the Appendix). More precisely, in the transmitted region the mode field profile shows the same transverse mode profile as that of input region. In other words, there is no mode conversion and the eigenmode profile is kept even if the light propagates through right-angle bent waveguide.

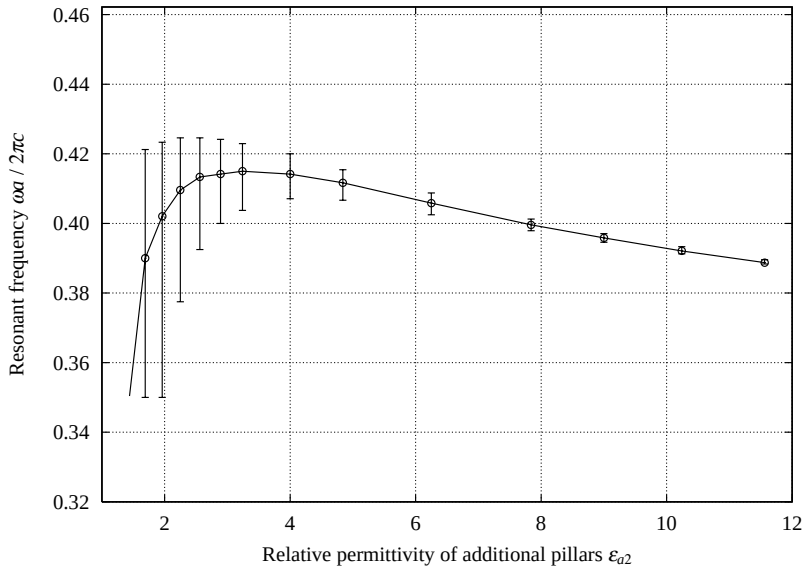


**Figure 4.** Resonant frequencies as a function of relative permittivity of additional pillars $\varepsilon_{a2}$ of L-shaped bent waveguide. Error bars denote frequency range whose reflected power loss is less than 0.2dB. The radii of additional pillars are fixed as $r_{a2}/a = 0.175$.

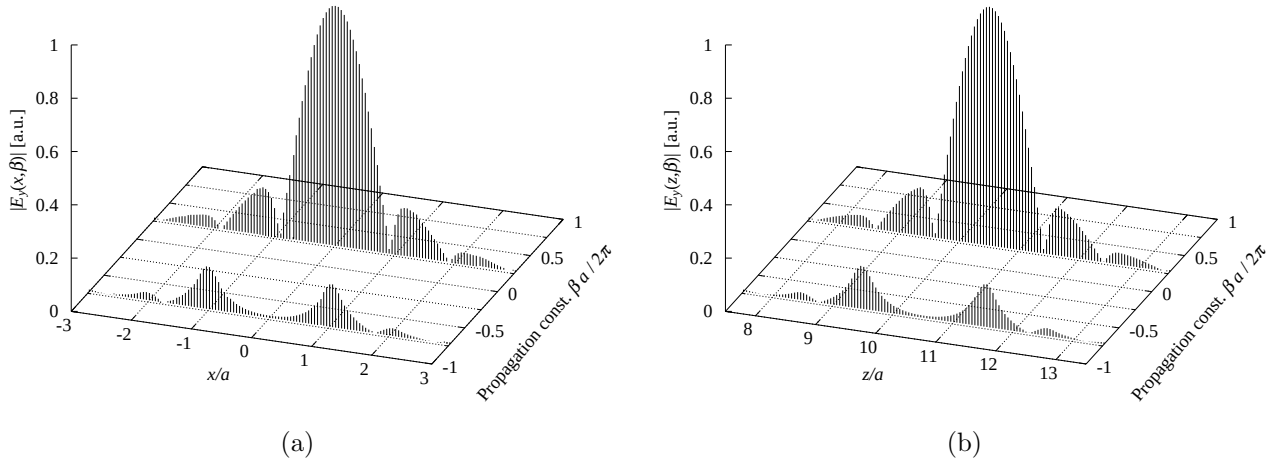


(a) (b)

**Figure 5.** Electric field intensity $|E_y|$ as a function of propagation constant $\beta$ for (a) input side and (b) output side of the L-shaped bent waveguide at the resonant frequency $\omega a/2\pi c = 0.389$.

# 3. Design of a Wavelength Multi/Demultiplexer

Using the L-shaped bent waveguides and the directional couplers we can design compact size wavelength multi/demultiplexer as shown in Figure 6. The number of channels of wavelength multi/demultiplexer determines the number of directional couplers, i.e., $M$-wavelengths are multi/demultiplexed by using $(M-1)$ directional couplers which are connected sequentially. As an example, we design three-wavelength multi/demultiplexer using two directional couplers. The directional coupler is composed of two waveguides which are single mode waveguide whose width is $W/a = 1.65$. The interval between two waveguides is $d/a = 0.35$ which corresponds one row of crystals.

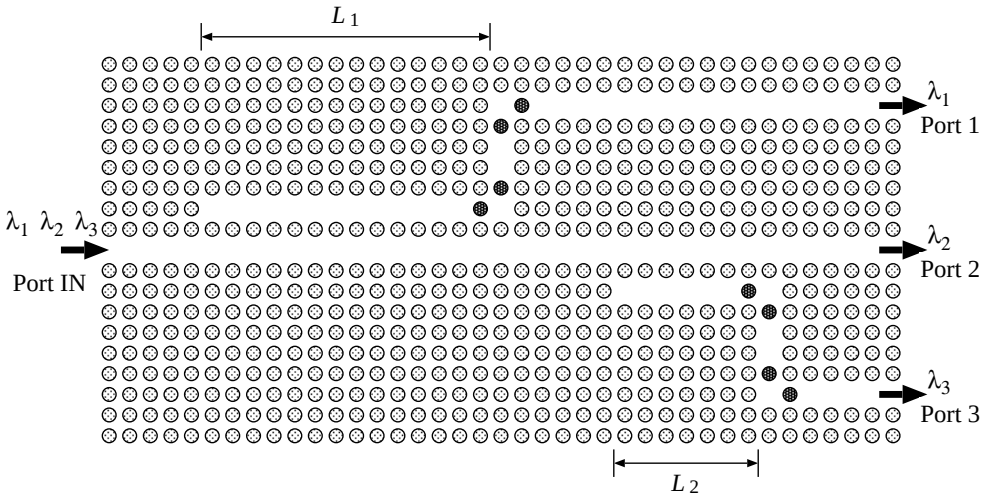


**Figure 6.** The structure of three-wavelength multi/demultiplexer. Black circles denote additional pillars whose radii and relative permittivity are $r_{a2}/a = 0.175$ and $\varepsilon_{a2} = 1.69$, respectively. Lengths of coupling region are $L_1/a = 48.0$ and $L_2/a = 24.0$, respectively. The parameters of photonic crystal $r_a/a = 0.175$ and $\varepsilon_a = 11.56$ are used.

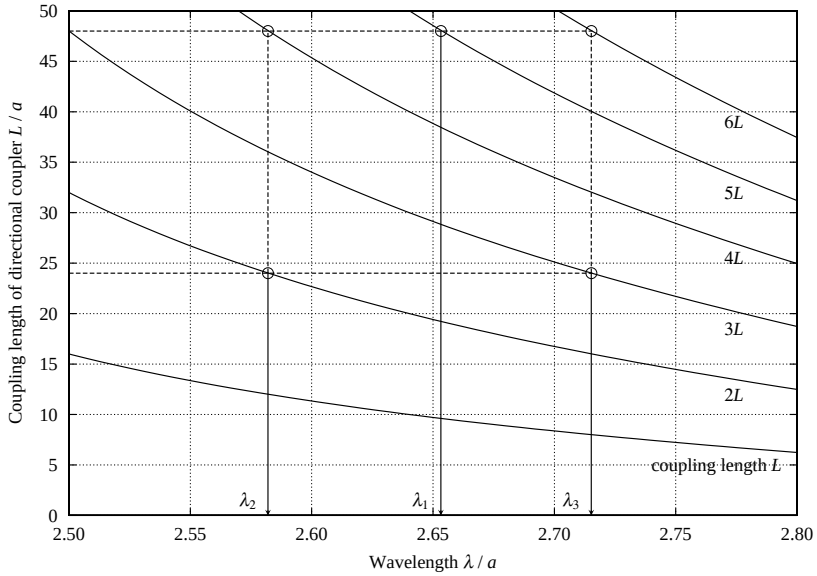


**Figure 7.** Coupling length of the directional coupler as a function of wavelength. The directional coupler is composed of two waveguides which are single mode waveguide whose width is $W/a = 1.65$. The interval between two waveguides is $d/a = 0.35$.

Before analyzing the device, we estimate design parameter of directional coupler. Figure 7 shows the normalized coupling length of the directional coupler $L/a$ as a function of wavelength. In the figure integral multiples of coupling length $nL(n = 1, 2, 3, \ldots)$ are plotted for determining the length of directional coupler. If the length of directional coupler is chosen as even-numbered multiples of the coupling length $2nL(n = 1, 2, \ldots)$, the optical power for appropriate wavelength is finally transmitted to straight port. Considering desired wavelengths which are filtered by the directional couplers, we choose the lengths of first

and second directional couplers as $L_1/a = 48$ and $L_2/a = 24$, respectively. From Figure 7 we can see that the light of wavelength $\lambda_1(= 2.66a)$ is completely transmitted to cross port of the first directional coupler and two different lights of wavelength $\lambda_2(= 2.58a)$ and $\lambda_3(= 2.72a)$ which are firstly transmitted to straight port of the first directional coupler are finally divided into two output ports through the second directional coupler.

Using these parameters we assemble directional couplers and L-shaped bent waveguides into the three-wavelength multi/demultiplexer as shown in Figure 6. In the corner region we place additional pillars denoted by black circles in the figure. In order to obtain wide transmission frequency characteristics, we choose the radii and relative permittivity of additional pillars as $r_{a2}/a = 0.175$ and $\varepsilon_{a2} = 1.69$, respectively. Transmission spectra of the three-wavelength multi/demultiplexer are shown in Figure 8. Here we evaluate the characteristics of three-wavelength multi/demultiplexer quantitatively by using the extinction ratio and insertion loss defined by

$$\text{Extinction ratio} = -10\log\left(\frac{P_i'}{P_i}\right) \quad , \quad \text{Insertion loss} = -10\log\left(\frac{P_i}{P_{\text{in}}}\right) \tag{3}$$

where $P_{\text{in}}$ is input power flow, $P_i$ and $P_i'$ indicate output power at port $i$ for a selected port and an unselected one, respectively. In fact extinction ratio and insertion loss for ports 1, 2, and 3 are almost greater than 17.9dB and less than $8 \times 10^{-2}$ dB, respectively as shown in the Table. We can see from the figure and table that additional pillars to right-angle bends realize high extinction ratio and low-insertion-loss. Figure 9 shows electric field intensity of the directional coupler for wavelength $\lambda/a = 2.66, 2.58$ and $2.72$. We can see that low-insertion-loss and high-extinction radio three-wavelength multi/demultiplexer whose overall length is approximately $35\lambda_m$, where $\lambda_m$ is a maximum wavelength of incident wave, can be realized in all incident wavelengths.

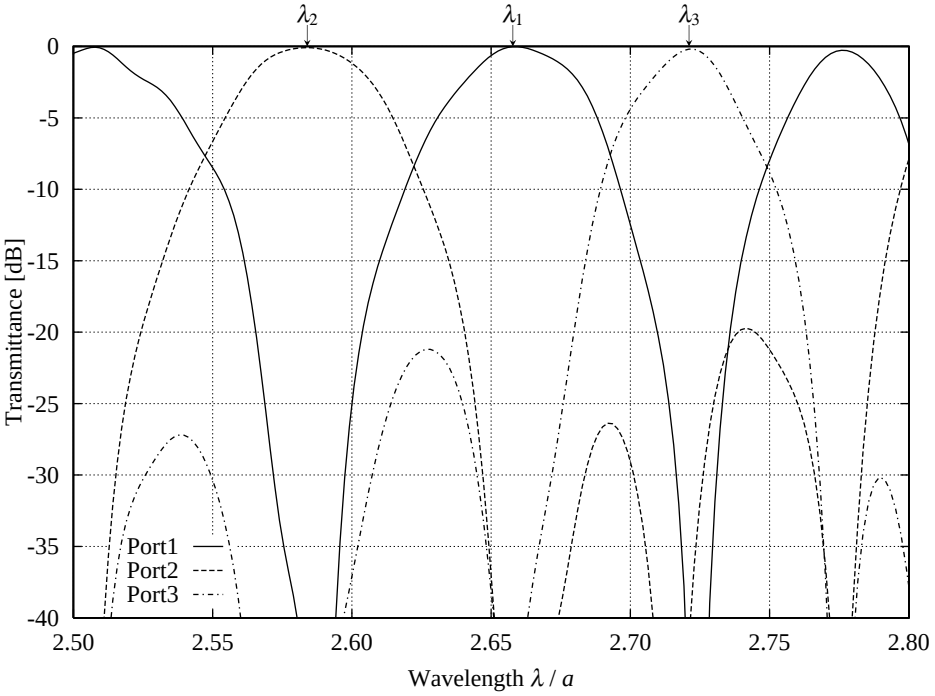


**Figure 8.** Transmission spectra of the three-wavelength multi/demultiplexer.

**Table** Extinction ratio and insertion loss of the three-wavelength multi/demultiplexer.

| wavelength $\lambda/a$ | extinction ratio [dB] | insertion loss [dB] | output |
|---|---|---|---|
| 2.66 | >20.6 | $6.4\times10^{-3}$ | Port 1 |
| 2.58 | >20.5 | $3.8\times10^{-2}$ | Port 2 |
| 2.72 | >17.9 | $8.1\times10^{-2}$ | Port 3 |

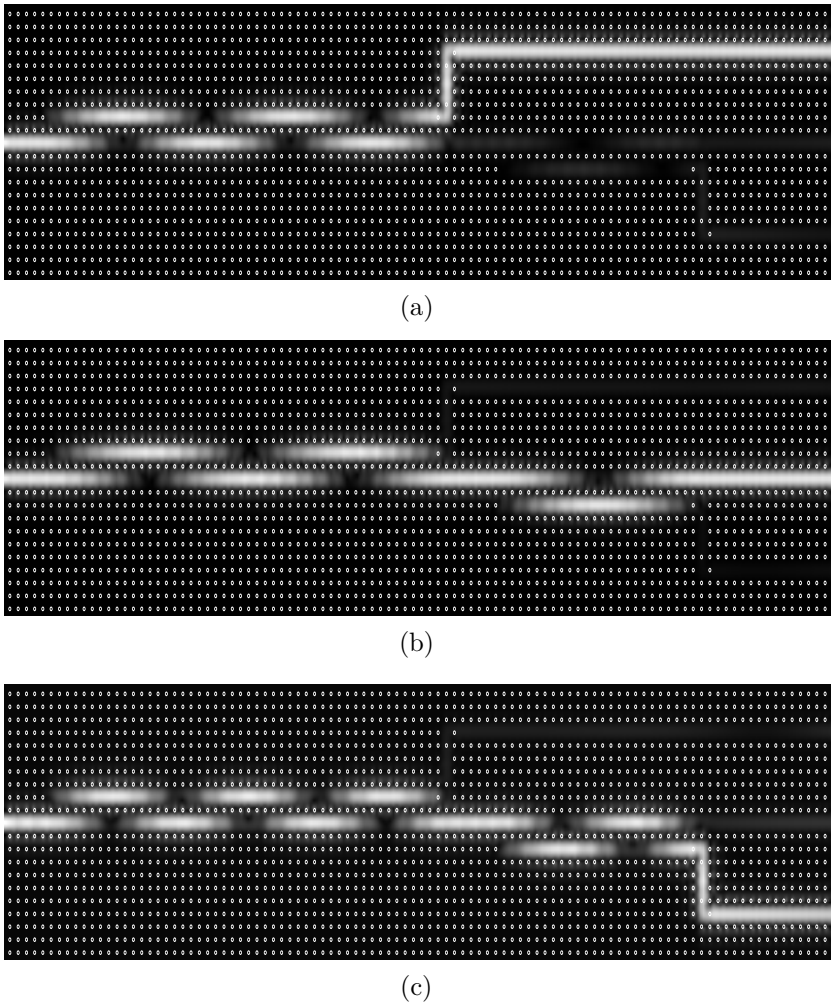

(a)

(b)

(c)

**Figure 9.** Electric field intensity of the three-wavelength multi/demultiplexer. (a) $\lambda/a = 2.66$. (b) $\lambda/a = 2.58$. (c) $\lambda/a = 2.72$.

# 4. Conclusion

We have proposed an excellent L-shaped bent waveguides composed of two-dimensional photonic crystal and analyzed its characteristics using the FDTD method based on the principles of MD-WDFs. Numerical results show that reflected waves from the right-angle corner can be completely eliminated by adding additional pillars due to resonant tunneling and its transmission bandwidths can be controlled by changing parameters of additional pillars. Using the L-shaped bent waveguides and directional couplers, we have designed the multi/demultiplexer and demonstrated that it can work as a low-insertion-loss device whose size is of the

order of the wavelength of light. From these results, we can conclude that the photonic crystal optical waveguide is a candidate of basic elements for constructing high density integrated optical circuits.

The waveguide devices constructed by the air-hole type photonic crystal [2] and the sensitivity of the performances of photonic crystal devices to defects and tolerances in the fabrication process which is one of the key issues for designing practical devices will be studied in the near future.

# References

[1] E. Yablonovitch, "Inhibited Spontaneous Emission in Solid-State Physics and Electronics", Physical Review Lett., **vol.58**, pp. 2059–2062 (1987).

[2] J.D.Joannopoulos, P.R.Villeneuve and S.Fan, "Photonic crystals: putting a new twist on light", Nature, **vol.386**, pp. 143–149 (1997).

[3] S.Y.Lin, E.Chow, V.Hietala, P.R.Villeneuve and J.D.Joannopoulos, "Experimental Demonstration of Guiding and Bending of Electromagnetic Waves in a Photonic Crystal", Science, **vol.282**, pp. 274–276 (1998).

[4] S.Fan, P.R.Villeneuve, J.D.Joannopoulos and H.A.Haus, "Channel Drop Tunneling through Localized States", Physical Review Lett., **vol.80**, pp. 960–963 (1998).

[5] H.Ikuno, Y.Naka and A.Yata, "Analysis of optical waveguide devices using the FDTD method based on the principles of multidimensional wave digital filters", Radio Science, **vol.35**, pp. 595–605 (2000).

[6] Y.Naka and H.Ikuno, "Guided mode analysis of two-dimensional photonic crystal optical waveguides", Proceedings of the 2000 Japan-China Joint Meeting on Optical Fibre Science and Electromagnetic Theory, Osaka, Japan, pp. 78–81 (2000).

[7] Y.Naka and H.Ikuno, "Analysis of 2-D photonic crystal L-shaped optical waveguide and its application to optical devices", Proceedings of 2001 URSI International Symposium on Electromagnetic Theory, Victoria, Canada, pp. 529–531 (2001).

[8] K.Takano and K.Nakagawa, "Frequency Analysis of Wavelength Demultiplexers and Optical Filters with Finite 2-D Photonic Crystals", IEICE Trans. Electron., **vol.E84-C**, pp. 669–677 (2001).

[9] J. Wang and H. Guo, "Resonant tunneling through a bend in a quantum wire", Appl. Phys. Lett., **vol.60**, pp. 654–656 (1992).

[10] A.Fettweis, "Wave Digital Filters: Theory and Practice", Proc. IEEE, **vol.74**, pp. 270–327 (1986).

[11] A.Fettweis, "Multidimensional Wave Digital Filters for Discrete-Time Modelling of Maxwell's Equations", Int. J. Numerical Modelling, **vol.5**, pp. 183–201 (1992).

[12] Y.Naka, H.Ikuno, M.Nishimoto and A.Yata, "FDTD Method with PMLs ABC Based on the Principles of Multidimensional Wave Digital Filters for Discrete-Time Modelling of Maxwell's Equations", IEICE Trans. Electron., **vol.E81-C**, pp. 305–314 (1998).

[13] J.P.Berenger, "A perfectly matched layer for the absorption of electromangetic waves", J. Computational Phys., **vol.114**, pp. 185–200 (1994).

[14] W.L.Ko and R.Mittra, "A Combination of FDTD and Prony Methods for Analyzing Microwave Integrated Circuits", IEEE Trans. Microwave Theory Tech., **vol. MTT-39**, pp. 2176–2181 (1991).

# Appendix

## A. Guided Mode Analysis

In order to design waveguide devices, we characterize the guided mode in the photonic crystal waveguides whose waveguide layer is constructed by removing one row of pillars. Figure A-1 shows electric field intensities and the Poynthing vector of photonic crystal waveguides. The parameters of photonic crystal $r_a/a = 0.175$ and $\varepsilon_a = 11.56$ are chosen. The waveguide width is $W/a = 1.65$, and the time harmonic wave is taken for incident wave such that

$$\psi(x, z = 0, t) = \psi_0(x) \sin(\omega t) \tag{A-1}$$

where $\psi_0(x)$ denotes a transverse profile which is a truncated cosine and $\omega$ is angular frequency. The frequency of incident wave is $\omega a/2\pi c = 0.40$. Circles in these figures denote positions of pillar. We can see that electric field intensities oscillate along with an array of pillars in the propagation direction $z$ and optical power made vortices near the crystals located boundary between waveguide layer and cladding layer. Spatial profiles of electric field intensities $|E_y|$ as a function of wavenumber in $z$ direction $k_z$ are shown in Figure A-2. Spatial wavenumber profiles are calculated by the Prony's method [14]. In this method spatial profiles of electric field in the waveguide can be approximated by sums of complex exponentials. Here we expand electric field profile expressed by 120 data points along $z$ direction into 40 terms of complex exponentials. From these figures we can see that there are two wavenumbers of fundamental mode $(\beta_0, \beta_0 - 2\pi/a)$. It is noted that this fact can be checked for higher order modes of this type of photonic crystal waveguide. Then we can intuitively express the complex electric field in the photonic crystal waveguide $E_y^m(x, z)$ for any guided mode $m$ as follow:

$$\begin{aligned} E_y^m(x, z) &= \psi_1^m(x) e^{-j\beta_m z} + \psi_2^m(x) e^{-j(\beta_m - 2\pi/a)z} \\ &= \left[\psi_1^m(x) + \psi_2^m(x) e^{j2\pi z/a}\right] e^{-j\beta_m z} \end{aligned} \tag{A-2}$$

where the time dependence $\exp[j\omega t]$ will be assumed, and $\psi_1^m(x)$ and $\psi_2^m(x)$ denote transverse electric field profile whose wavenumber are $\beta_m$ and $(\beta_m - 2\pi/a)$, respectively. From this representation we can find that electric field intensities of photonic crystal waveguides propagate with a propagation constant $\beta_m$ and oscillate in the period of lattice constant $a$ as described in $\left[\psi_1^m(x) + \psi_2^m(x) e^{j2\pi z/a}\right]$. In fact we can calculate the dispersion relation of the fundamental mode of the photonic crystal waveguides as shown in Figure A-3. The waveguide width is $W/a = 1.65$. From Figure A-3 we can see that only fundamental mode $\beta_0$ exists in the waveguide.

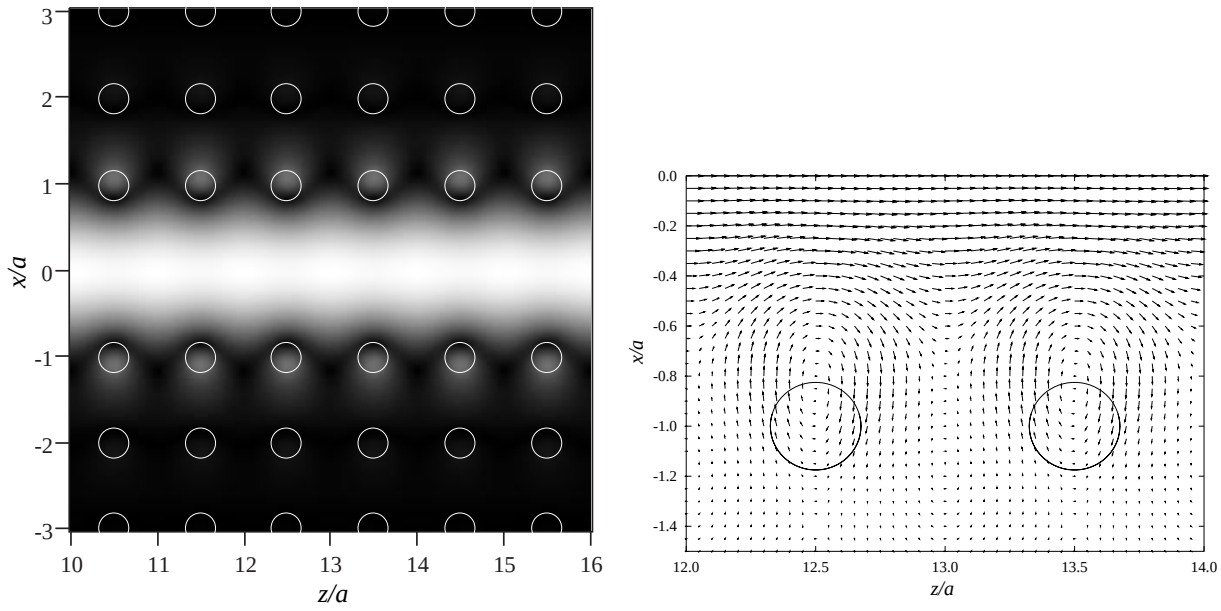


(a) (b)

**Figure A-1.** Electric field intensity and Poynting vector of photonic crystal waveguide. The waveguide width and incident frequency are $W/a = 1.65$ and $\omega a/2\pi c = 0.40$, respectively. (a)Electric field intensity. (b) Poynting vector.

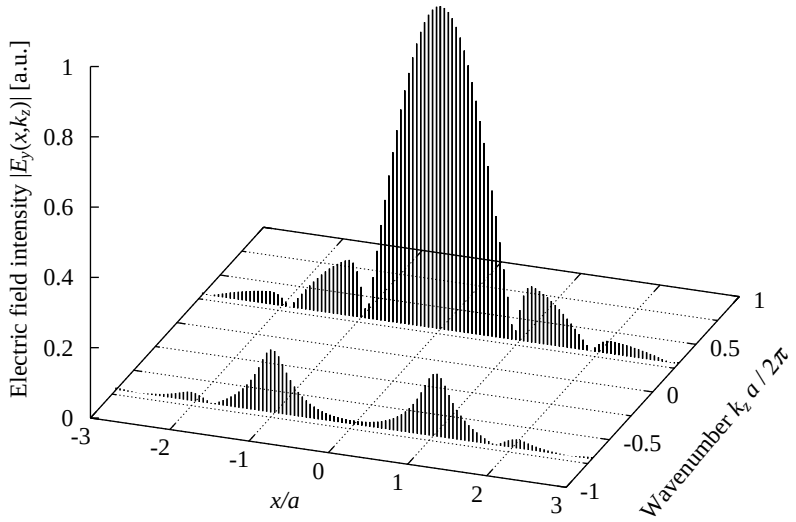


**Figure A-2.** Electric field intensity $|E_y|$ as a function of wavenumber in propagation direction $k_z$. The incident frequency is $\omega a/2\pi c = 0.40$, and the waveguide width is $W/a = 1.65$.

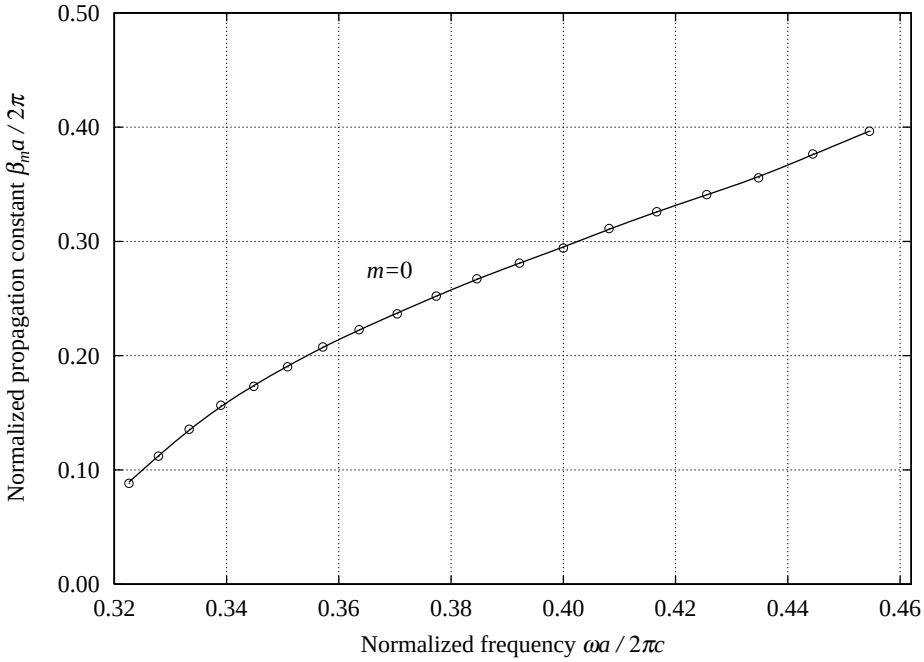


**Figure A-3.** Dispersion relation of the fundamental mode of photonic crystal waveguides. The waveguide width is $W/a = 1.65$.